Influence of subpicosecond laser pulse duration on proton acceleration

M. Carrié, E. Lefebvre, A. Flacco, and V. Malka

Citation: Physics of Plasmas **16**, 053105 (2009); doi: 10.1063/1.3138742
View online: http://dx.doi.org/10.1063/1.3138742
View Table of Contents: http://scitation.aip.org/content/aip/journal/pop/16/5?ver=pdfcov
Published by the AIP Publishing

Influence of subpicosecond laser pulse duration on proton acceleration

M. Carrié,[1,a)] E. Lefebvre,[1] A. Flacco,[2] and V. Malka[2]
[1]*CEA, DAM, DIF, Bruyères-le-Châtel, 91297 Arpajon, France*
[2]*Laboratoire d'Optique Appliquée, ENSTA, CNRS, Ecole Polytechnique, UMR 7639, 91761 Palaiseau, France*

(Received 17 November 2008; accepted 23 April 2009; published online 19 May 2009)

The influence of pulse duration on proton acceleration using subpicosecond (30–300 fs), ultraintense (from 3.6×10^{18} to 3.6×10^{19} W/cm^2), constant energy (0.14 J) laser pulses is studied using two-dimensional simulations. The entire pulse duration is modeled so that during the rising edge of the pulse a preplasma can naturally expand from the target front and rear surfaces into vacuum, altering respectively laser absorption and electrostatic field generation. In this paper, we study this effect for two target profiles (sharp-edge profile and smooth density gradient at the front side) and we point out the existence of a weak optimum pulse duration for proton acceleration. For the different pulse durations we consider, we first show that the maximum proton energy variations are similar to those of the rear side electrostatic field amplitude. The energy variations, however, are smaller than expected from the field variations, and we explain this effect by characteristic proton acceleration time. © *2009 American Institute of Physics*. [DOI: 10.1063/1.3138742]

I. INTRODUCTION AND MOTIVATION

In the last decades, improvements in the laser chirp pulse amplification technology have allowed the construction of powerful laser facilities able to deliver on target focused intensities up to several 10^{21} W/cm^2. These intense laser beams can be used to efficiently accelerate high quality proton or ion beams off the rear surface of thin solid targets. These particle beams are laminar,[1] collimated[2] (micron size sources), and the maximum particle energy can reach several tens of MeV per nucleon. They can be used in a wide range of applications such as imaging in plasma physics,[3] the study of warm dense matter,[4] or in the medical field with proton therapy.[5]

In the current laser parameters state of art, 10^{18} to several 10^{21} W/cm^2 laser beams can be achieved, and the ion acceleration mechanism, known as target normal sheath acceleration,[6] is relatively well understood. When the incident laser beam impinges on the front surface of a thin solid target, an evanescent wave tunnels inside the target over several skin depths. The resulting ponderomotive force pushes the electrons away from the laser high intensity regions. Other mechanisms can also transfer the incident laser energy to electrons such as Brunel effect, $\vec{j}\times\vec{B}$ heating, and resonant absorption.[7,8] These relativistic electrons transport through the thin target. They come out at the rear side, expand into vacuum, and set up an electrostatic sheath at this surface, accelerating protons or heavier ions to multi-MeV energy over a distance of several micrometers.

How the maximum proton or ion energy varies with target and laser's parameters is a complex question depending on many parameters such as laser irradiance, pulse duration, laser energy, absorption efficiency, target thickness, and density. The effect of laser intensity on the maximum proton energy has already been studied by a number of authors: in 2000, Maksimchuk *et al.*[9] studied the dependence of maximum proton energy with laser intensity in the range of 10^{17}–3×10^{18} W/cm^2 and a fixed laser pulse duration (400 fs). They observed a dependence with intensity proportional to I^{α} with α between 0.3 and 0.4. Oishi *et al.*[10] conducted experiments with laser intensity varying from 8.5×10^{17} to 1.1×10^{19} W/cm^2 and the laser pulse duration from 55 to 400 fs. For a fixed laser pulse duration of 55 fs, they reported a maximum proton energy variation with intensity in agreement with Mora's model[11] when the effective proton acceleration time scales as the laser pulse duration. Sentoku *et al.*[12] studied this problem with numerical simulations and obtained a maximum proton energy dependence $\propto I$ at subrelativistic intensities and $\propto I^{0.5}$ at high intensities. Another relevant question in studies of proton or ion acceleration is the optimization of particle acceleration for a fixed incident laser energy. This is especially legitimate from an experimental perspective, as the overall pulse energy is often bounded, but the pulse duration can be more easily varied. Indeed, one can imagine that very short and intense pulse will generate a relatively small number of very energetic electrons. On the contrary, we expect a large number of less energetic electrons from a lower-intensity, longer-duration pulse. How the acceleration varies between these two limits is still an open question. Additional effects such as variations in the absorption with laser intensity, or perturbation of the target back surface by the laser prepulse, or target preheating by the rising edge of the pulse will likely affect the position of the pulse duration optimum for the maximum proton or ion energy between these two limits for a fixed incident laser energy.

Several simplified models[11,13] have been proposed that try to relate the interaction parameters (laser and target characteristics) to the peak proton energy. But the existence of many free parameters (such as the relationship between intensity and electron temperature, uncertainties on the electron beam divergence, on the laser energy absorption which

a)Electronic mail: michael.carrie@cea.fr.

can depend sensitively on the interaction conditions) limits their predictivity.

In this article, we use direct numerical simulations with a two-dimensional (2D) particle-in-cell (PIC) code to study the variations in proton acceleration with pulse duration for a fixed laser energy. In Sec. II, we present the numerical setup of our simulations. In Sec. III, we show the numerical results for two target geometries (one with sharp edge and the other with a smooth density gradient at the front side). In Sec. IV, we try to relate the maximum proton energy variations with the electrical field measured at the rear side through scaling laws including the characteristic density gradient length at the rear side. We show that the pulse duration triggers three direct consequences which influence the maximum proton energy: the characteristic gradient length at the rear side, the characteristic time of energy exchange between protons and electrons, and the laser absorption rate. Overall we observe relatively moderate variations in the peak proton energy with pulse duration when the laser energy is held fixed. This weak dependence is found to result from stronger but conflicting variations of the above-mentioned parameters.

II. NUMERICAL SETUP

In order to study the effect of pulse duration on the maximum proton energy, we carried out a set of 2D simulations using the PIC code CALDER.[14] In these simulations, we used a short (subpicosecond), intense (larger than 10^{18} W/cm^2), *p*-polarized laser pulse with a wavelength of 800 nm. The laser pulse is emitted from the left side of the simulation box with an incidence angle of 45° on target and a focal spot of 2.8 μm. The pulse intensity is modeled with a Gaussian shape. The full width at half maximum (FWHM) τ_p varies from 30 to 300 fs. The pulse energy is kept constant and equal to 0.14 J. Consequently, the intensity goes from 3.6×10^{19} to 3.6×10^{18} W/cm^2. The peak intensity enters the box at a time t equal to 1.83 times the FWHM, so that the rising edge of the main pulse can be fully described. In our simulations, we used two target density profiles consisting of a sharp-edge target with a 3 μm homogeneous density at $50n_c$ and a smooth-edge target with an exponential preplasma at the front side of the form $n_e(x)=50n_c\times\exp(-x/l_{ss})$. l_{ss} is the characteristic gradient length and the preplasma density goes from 1% to 100% of $50n_c$ over $4.6l_{ss}$. The target is assumed to be completely ionized hydrogen and is placed in a simulation box of 56×38 μm^2. The collisional effects are not taken into account as electrons are relativistic in our study and the thin target behavior we investigate is dominated by collective fields.[15] The plasma is sampled initially with 100 particles per target cell and per species (electrons and protons). The time step and grid size are 0.027 fs and 11 nm, respectively. We used a third-order interpolation scheme to compute the densities and currents on each grid node in order to keep numerical heating to a value where it does not affect the results. The boundary conditions are periodic in transverse and absorbing in longitudinal directions for the fields and absorbing/reinjecting for the particles[16] to ensure the quasineutrality inside the box.

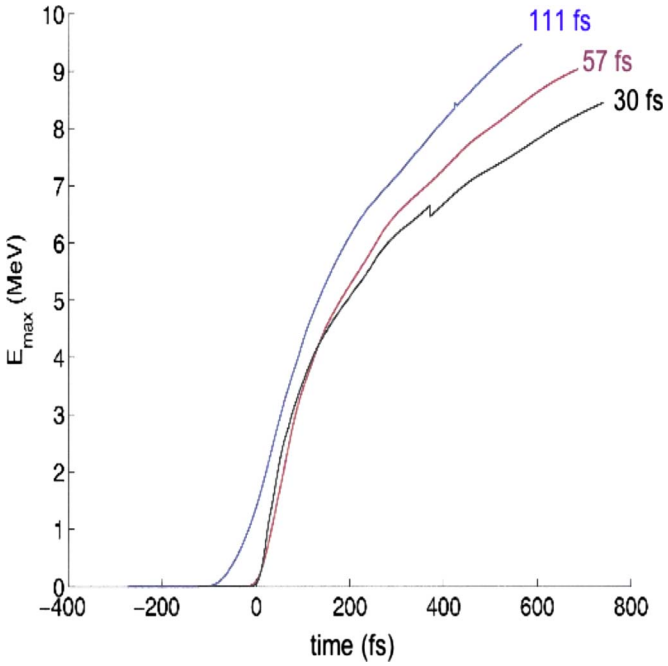

FIG. 1. (Color online) Evolution of the maximum proton energy with time for τ_p=30, 57, and 111 fs.

III. RESULTS

A. Sharp-edge target

The evolution of peak proton energy with time for several laser pulse durations is plotted in Fig. 1 using as a common reference t=0, the time at which the peak of the laser pulse reaches the initial front target surface. The maximum proton energy corresponds to the cutoff position in the energy spectrum and varies with time. As apparent in this figure, all simulations have been run to roughly 600 fs, a point where we are confident that subsequent evolution of ion peak energy will not qualitatively change the ordering of the curves. For all pulse durations we consider, we plot in Fig. 2(a) the maximum proton energy at t=500 fs and the laser absorption as a function of τ_p. We notice an increase in the maximum energy and the absorption with the laser pulse duration. For long pulse durations, absorption saturates around 70% of the incident laser energy and the maximum proton energy increases slightly from 7 to 10 MeV between τ_p=30 and 219 fs, then decreases slowly as the pulse duration becomes longer. During the rising edge of the pulse, significant electron heating starts around $\sim10^{17}$ W/cm^2 and the hot electrons expand around the target. At the target front surface, this expansion leads to a smoother density profile which favors higher absorption of the trailing pulse.[17] As shown in Fig. 2(a), absorption increases from 22% for the shortest pulse duration to 70% for τ_p=300 fs. To draw meaningful conclusions regarding ion acceleration, it is interesting that absorption should have limited variations: we therefore considered a different target profile, adding a preplasma at the front side to increase the absorption of the shortest pulses.

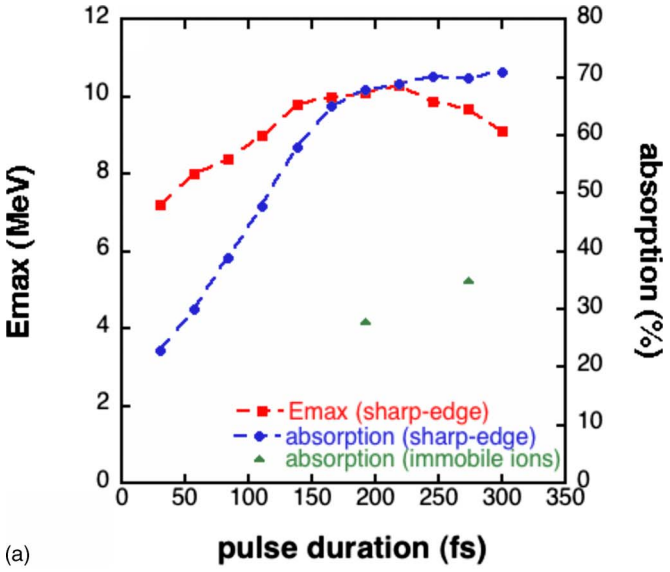

(a)

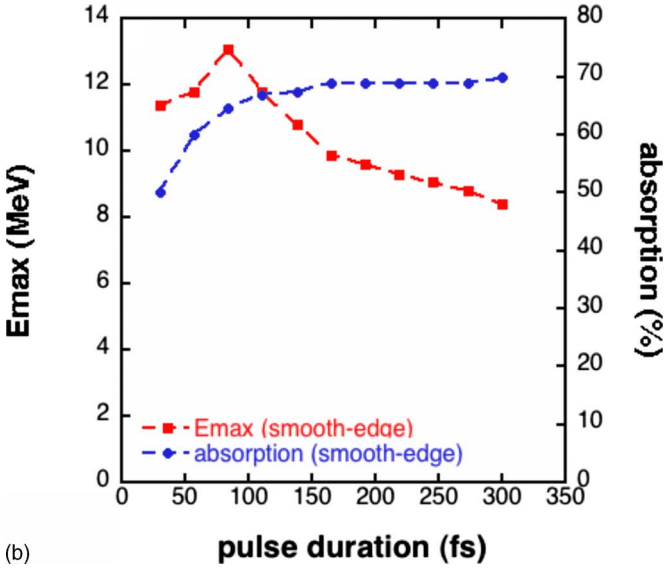

(b)

FIG. 2. (Color online) (a) Sharp-edge and (b) smooth-edge target maximum proton energy and laser absorption vs pulse duration.

B. Scaling with gradient length

For these simulations, we use a smooth-edge target with an exponential preplasma at the front side of the form $n_e(x)=50n_c\times\exp(-x/l_{ss})$. The amount of matter added with the preplasma is small compared to the homogeneous part. Therefore, we are able to compare the hot electron density in both target profiles, even though the homogeneous part is kept identical to the sharp-edge target. That is why the homogeneous part is kept identical to the previous target. The characteristic gradient length l_{ss} varies from 100 to 600 nm. The maximum proton energy and the absorption as a function of the gradient length at the front side of the target are reported in Fig. 3 for the shortest pulse duration (30 fs).

The highest proton energy is obtained for a gradient length of 200 nm. The corresponding absorption is about 50% of the incident laser energy. For longer gradient lengths, the absorption does not evolve significantly and remains close to 50%. As long as gradients are time consuming because the number of particles to compute is increased, we choose $l_{ss}=200$ nm in order to limit both the calculation time and the variations in absorption.

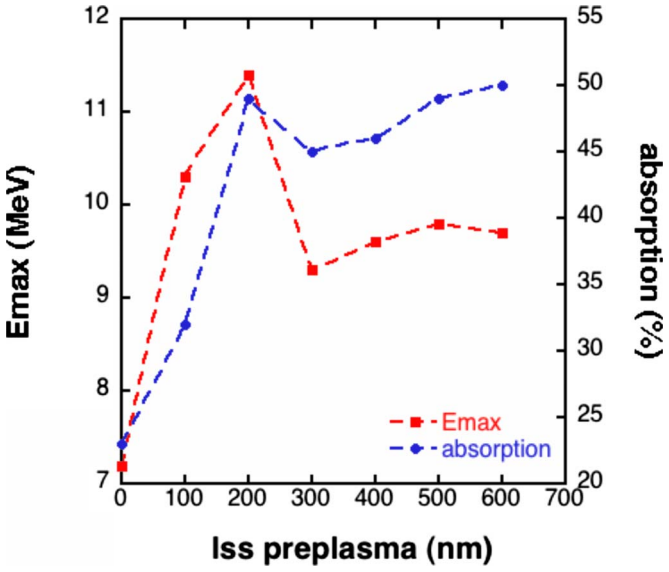

FIG. 3. (Color online) Maximum proton energy and absorption variations vs gradient length for the 30 fs laser pulse duration.

C. Smooth-edge target

We carried out the same set of simulations as the sharp-edge target but with the addition of the 200 nm gradient length preplasma at the front side. The maximum proton energy and the absorption versus the pulse duration are shown in Fig. 2(b). The preplasma at the front side increases the absorption for the shortest pulse durations (from 20% to 50%). The absorption now varies from 50% for $\tau_p=30$ fs to 70% for $\tau_p=300$ fs. As expected, the maximum proton energy increases compared to the sharp-edge target case for the shortest pulses. For longer pulses the two data sets show very similar figures. The peak maximum proton energy is now reached for $\tau_p=84$ fs. The conversion efficiency of the incident laser energy into proton kinetic energy is plotted in Fig. 4. It represents the fraction of incident laser energy converted into the total (crosses) and superior to 4 MeV (circles) forward proton kinetic energy for the sharp and smooth-edge profiles. Our efficiency measurements for the forward proton kinetic energy above 4 MeV is in agreement with experiments where it was found to be about 10^{-3} for similar laser parameters.[13] It is noteworthy that even though the laser absorptions that we compute are rather large, the laser-to-proton conversion efficiencies are close to measured values.

IV. DISCUSSIONS

When the laser pulse duration increases, the front surface plasma heated by the rising edge of the pulse has more time to expand before the peak intensity hits the target. As the electron density gradient length increases at the front side, absorption increases[18] and more electrons are heated to high temperatures. This effect is clearly exhibited in Fig.

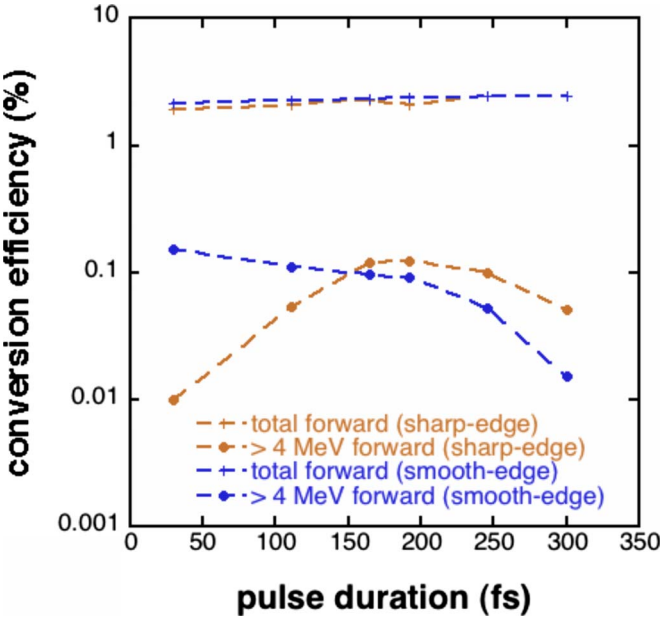

FIG. 4. (Color online) Conversion efficiency of the laser energy into proton kinetic energy.

2(a): indeed, we carried out simulations with immobile protons for the sharp-edge target and observed that absorption was reduced by a factor of 2 in this case.

The heated electrons travel through the target, come out at the rear side, and expand into the vacuum creating an electrostatic field which starts accelerating protons located at the back surface. Thus, protons begin to be accelerated before the arrival of the peak of the pulse. This preliminary proton acceleration from the back surface into vacuum creates a density gradient. This gradient is known to diminish the strength of the electrostatic field seen by the protons located at the back surface.[19,20] In Fig. 5, the back gradient length of proton density at the time of peak intensity L_{ss} is plotted as a function of the laser pulse duration for both target profiles. It can be seen that the gradient length increases with τ_p. This is related to the expansion time of protons which becomes larger when the laser pulse duration increases.

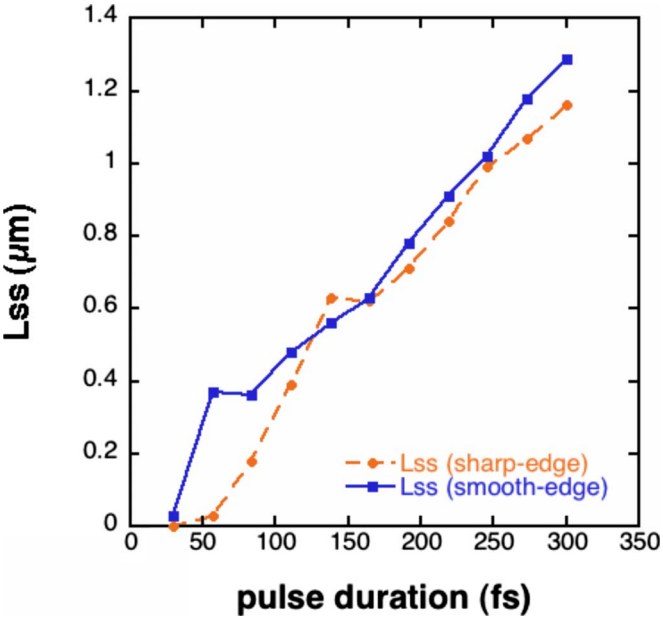

FIG. 5. (Color online) Gradient length at back surface vs pulse duration.

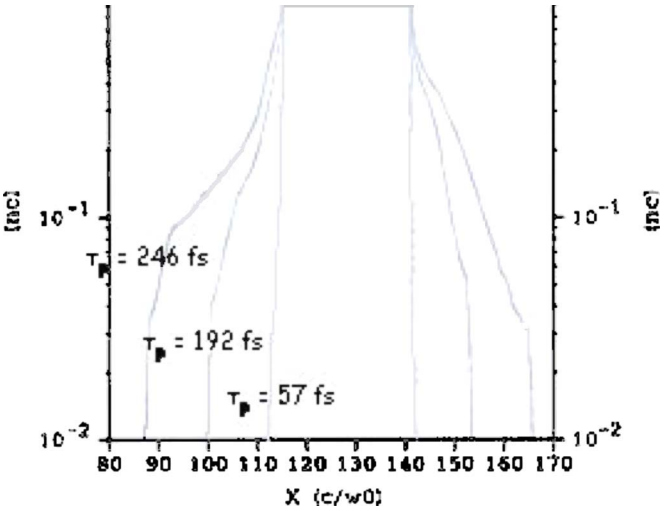

FIG. 6. (Color online) Snapshots of proton expansion at the time when the main pulse hits the front surface of the sharp-edge target for the τ_p=57, 192, and 246 fs simulations (the laser is incident from the left).

Figure 6 represents the proton density profile for three different pulse durations at the time when the peak of the pulse hits the target. The density gradient created at the rear side is clearly visible and should hamper proton acceleration according to Ref. 19. However one can notice from Figs. 2(a) and 2(b) that in both cases, the maximum proton energy first increases with τ_p before decreasing. We are facing a competition between absorption, rear side density gradient length, and the characteristic energy exchange time between protons and electrons.[21] While the gain in proton energy due to absorption is higher than the loss due to shielding at the rear surface, the maximum proton energy increases. On the contrary, when the energy gain due to absorption cannot overcome anymore the loss due to shielding, we observe a decrease in the maximum proton energy. This balance points out to the existence of an optimum pulse duration. This optimum is found to be relatively weak and depends on the details of the interaction: for instance, it varies from 84 to 219 fs when the target profile is changed in our calculations.

To give qualitative understanding of this balance, we plot in Figs. 7(a) and 7(b) the evolution of the hot electron temperature ($\geq$100 keV) and density measured when the peak intensity arrives on target as a function of τ_p. First of all, the temperature of hot electrons is expected to be close to the ponderomotive potential according to Wilks formula[18] $\varepsilon_h = m_e c^2(\sqrt{1+a_0^2}-1)$, where m_e is the electron mass, c is the speed of light, and a_0 is the normalized vector potential. This is what we observe in Fig. 7(a) for the longest pulse durations, i.e., the lowest values of a_0. However, for the shortest pulses, i.e., largest a_0, the rising edge of the laser pulse has little time to heat electrons before the arrival of the peak pulse. Therefore, the preplasma at the target front surface

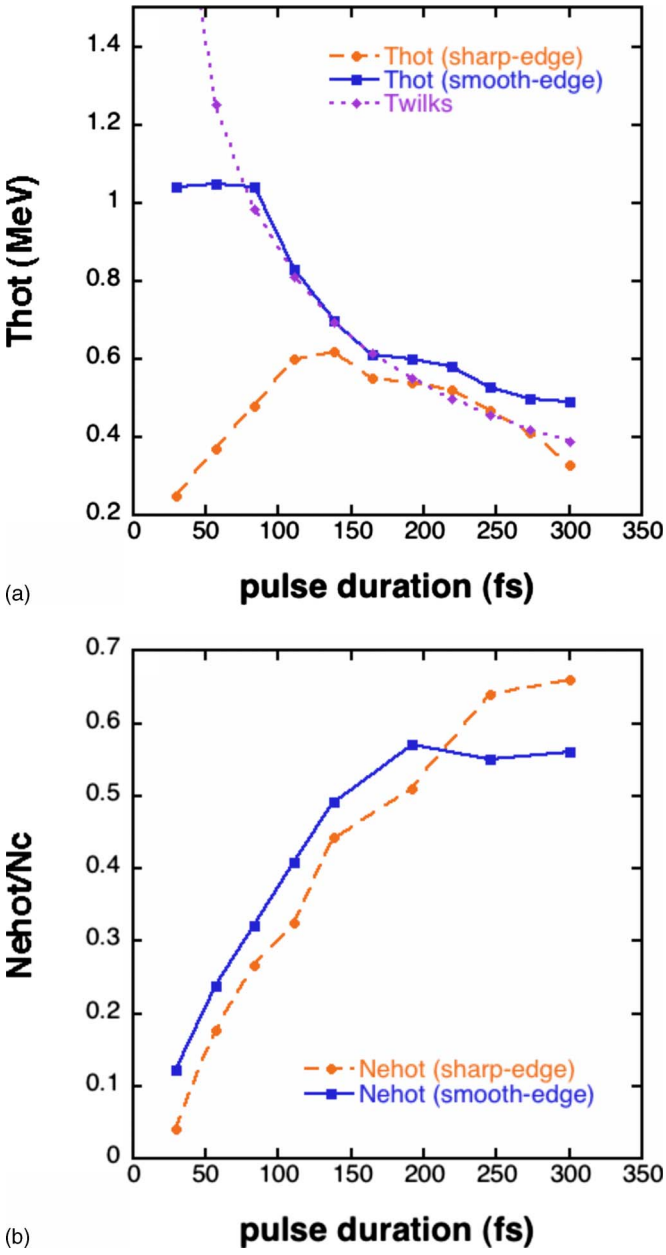

FIG. 7. (Color online) Evolution of the hot electron temperature and density with τ_p for both profiles.

cannot expand so much into vacuum so that the absorption is reduced and the hot electron temperature is below the Wilks approximation.[17] Consequently, we observe lower electron temperature for the shortest pulses. On the other hand, in the smooth-edge target, a preplasma is present from the beginning at the front side and we observe a higher absorption and hot electron temperature for the shortest pulses compared to the sharp-edge case. Then, in Fig. 7(b) the density of hot electron increases with the pulse duration. This behavior can be explained by the product $N_{\mathrm{hot}} \times T_{\mathrm{hot}}$ which represents the incident laser energy put into the hot electrons to be compared with the absorption (Fig. 2). First, in both cases, the absorption increases before it saturates. As the temperature of hot electrons increases for the sharp-edge target and is constant for the smooth-edge target, we observe an increase in the hot electron density for the shortest pulse durations. For longer pulses, the hot electron temperature gets close to Wilks' approximation and the absorption saturates. The density of hot electrons has to increase for the absorption to be constant. This is what we observe except for the longest pulses in the smooth-edge case where the temperature is reduced by 12% from τ_p=200 to 300 fs so that the evolution of hot electron density is less important than in the sharp-edge case where it is reduced by 37%.

The influence of the rear side gradient length, hot electron temperature, and absorption (through the hot electron density) on the maximum proton energy can be summarized by comparing the value of the electrostatic field measured at the rear side of the target and the electrostatic field computed from these three parameters when the peak intensity reaches the front side. It is expected that the electrostatic field E_x scales as $\sqrt{n_{\mathrm{hot}} T_{\mathrm{hot}}}$ when the density gradient length L_{ss} is small compared to the initial hot electron Debye length $\lambda_{D0} = (\varepsilon_0 k T_{\mathrm{hot}}/n_{\mathrm{hot}} e^2)^{1/2}$ and varies as T_{hot}/L_{ss} when $L_{ss} \gg \lambda_{D0}$.[6,11] Figure 8 represents the electrostatic field measured in the simulation box (circles) and the two scaling laws (blue/dark and yellow/light) as a function of τ_p for sharp-edge [Fig. 8(a)] and the smooth-edge cases [Fig. 8(b)]. It is clearly seen that the measured electrostatic field is a combination of these two scaling laws depending on the value of the density gradient length, i.e., of the pulse duration. In the preplasma case for the short pulse durations, the hot electron temperature is about 1 MeV, the hot electron density increases and the proton density gradient length at the rear side is too small to hamper proton acceleration. The peak in the maximum proton energy corresponds to the maximum electrostatic field. For longer pulse durations, the hot electron density keeps increasing while the hot electron temperature decreases continuously and the gradient length increases. Consequently, the maximum proton energy starts decreasing as the pulse duration increases for τ_p greater than 100 fs. In the sharp-edge case, we observe a similar variation in the electrostatic field with τ_p shifted to longer pulse durations, and we find this behavior reflected in the maximum proton energy variation. In both cases, we notice that the electrostatic field follows one scaling law or the other depending on the comparison between the density gradient length and the hot electron Debye length.

From Figs. 2(a), 2(b), and 8, it can be observed that the variations in the measured electric field are more important than the variations in the maximum proton energy. For instance, in the smooth-edge case, the electric field is reduced by a factor of about 2 between τ_p=165 fs and τ_p=300 fs, whereas the maximum proton kinetic energy is only decreased by a factor of about 1.2. If we simply consider the equation of motion for an ion, we have $dv \propto E_x dt$ and we therefore expect $E_{\max} \propto (E_x \tau_p)^2$. Indeed, between 165 and 300 fs, the $(E_x \tau_p)^2$ product varies by 1.25. In Fig. 9, the pulse duration τ_p=165 fs is taken as a reference. The squares represent the ratio $E_{\max}(\tau_p)/E_{\max}(165\ \mathrm{fs})$ so that the maximum proton energy is normalized to the 165 fs case. If the $E_{\max} \propto (E_x \tau_p)^2$ scaling is relevant, the curves representing $E_{\max}(\tau_p)/E_{\max}(165\ \mathrm{fs})$ and $[E_x(\tau_p)\tau_p/E_x(165\ \mathrm{fs})165\ \mathrm{fs}]^2$ should have the same variations. We observe that for short

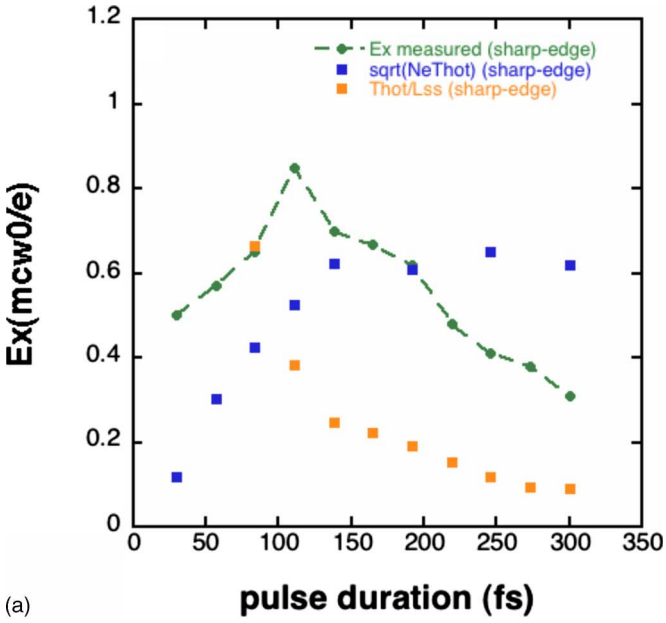

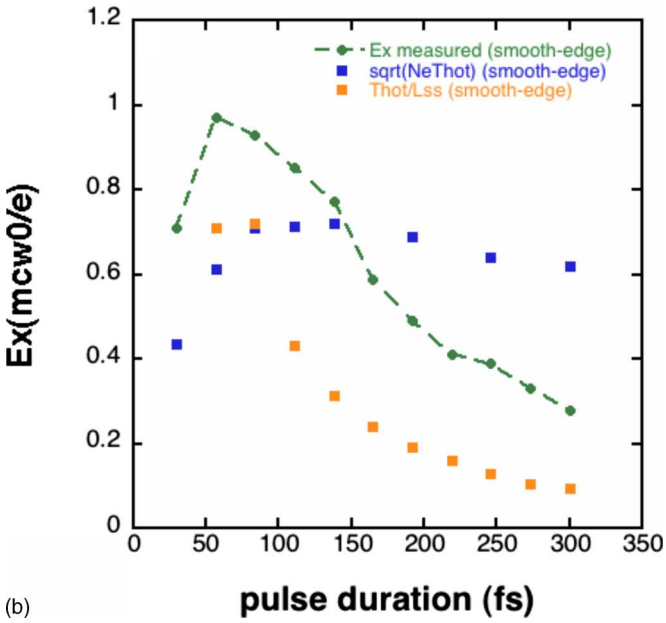

FIG. 8. (Color online) Electrostatic field measured and computed from the hot electron density, temperature, and the gradient length with τ_p for (a) sharp-edge and (b) smooth-edge profiles.

pulse durations, this scaling is not relevant: the peak proton energy it predicts underestimates the computed energy. On the contrary, for $\tau_p > 165$ fs, the curves are barely different which indicates that this scaling is adapted for long pulse durations. The explanation for this trend is that the characteristic time scale for the plasma evolution is the longest between heating (i.e., τ_p) and the energy exchange time between electrons and protons. For long pulse durations, this characteristic time scales as τ_p, and the $(E_x\tau_p)^2$ scaling is therefore relevant. For the shortest pulses, τ_p underestimates the characteristic time of the system and the $(E_x\tau_p)^2$ scaling (circles) underestimates the final proton energy (squares).

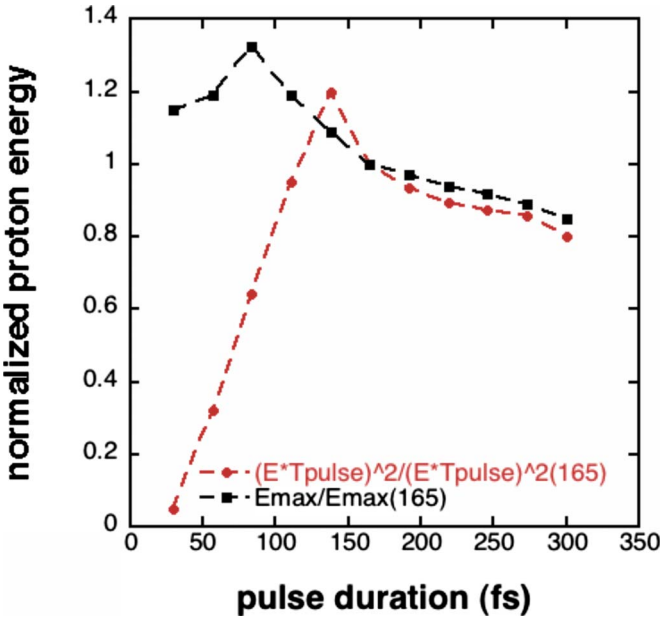

FIG. 9. (Color online) Variations in $E_{max}(\tau_p)/E_{max}(165\ \text{fs})$ (squares) and $[E_{elec}(\tau_p)\tau_p/E_{elec}(165\ \text{fs})165\ \text{fs}]^2$ (circles) with the pulse duration from 30 to 300 fs.

V. CONCLUSION

From this study of pulse duration influence on ion acceleration, we identified three processes which have an important influence on the maximum proton energy: the preplasma expansion at the front side of the target,[22] the early rear side expansion due to electron heating before the arrival of the pulse peak, and the acceleration time. The front surface expansion enhances absorption of long pulses. The electrostatic field at the rear side scales as $\sqrt{n_{hot}T_{hot}}$ when the density gradient length is smaller than the hot electron Debye length and varies as T_{hot}/L_{ss} when $L_{ss} \gg \lambda_{D0}$. This behavior is reflected in the scaling of the peak electrostatic field with pulse duration. Finally, the characteristic acceleration time was found to increase with the laser pulse duration, mitigating the reduction in peak proton energy with longer pulses. These three effects explain the existence of an optimum laser pulse duration. In the sharp-edge target, absorption is a rapidly growing function of pulse duration, and the maximum proton energy is weakly dependent on pulse duration. For the smooth-edge profile, we measure higher absorption even for short pulses, so that higher proton energy is obtained and the optimum pulse duration is shifted to shorter pulses.

From a practical point of view, it is now achievable with the development of plasma mirror[23] or cross-polarized wave (XPW) technics[24] to generate ultrahigh contrast pulses and we deduce from the above study that the optimum acceleration can be achieved by simultaneously controlling the pulse duration and the initial preplasma on the target front side using an auxiliary laser pulse.[22] We have shown that the optimum pulse duration for proton acceleration with fixed laser energy results from a balance between the absorption, the density gradient length effect, and the characteristic evolution time of the system. It is the first time to our knowledge that this effect which was reported experimentally for longer

pulses in the picosecond range[25] is demonstrated with direct numerical simulations for subpicosecond pulses.

[1] T. E. Cowan, J. Fuchs, H. Ruhl, A. Kemp, P. Audebert, R. Stephens, M. Roth, I. Barton, A. Blazevic, E. Brambrink, J. Cobble, J. Fernández, J.-C. Gauthier, M. Geissel, M. Hegelich, J. Kaae, S. Karsch, G. P. Le Sage, M. Manclossi, S. Letzring, S. Meyroneinc, A. Newkirk, H. Pépin, and N. Renard-LeGalloudec, Phys. Rev. Lett. **92**, 204801 (2004).

[2] J. Fuchs, T. E. Cowan, P. Audebert, H. Ruhl, L. Gremillet, A. Kemp, M. Allen, A. Blazevic, J.-C. Gauthier, M. Geissel, M. Hegelich, S. Karsch, P. Parks, M. Roth, and Y. Sentoku, Phys. Rev. Lett. **91**, 255002 (2003).

[3] M. Borghesi, D. H. Campbell, A. Schiavi, M. G. Haines, O. Willi, A. J. MacKinnon, P. Patel, L. A. Gizzi, M. Galimberti, R. J. Clarke, F. Pegoraro, H. Ruhl, and S. Bulanov, Phys. Plasmas **9**, 2214 (2002).

[4] P. K. Patel, A. J. Mackinnon, M. H. Key, T. E. Cowan, M. E. Foord, M. Allen, D. F. Price, H. Ruhl, P. T. Springer, and R. Stephens, Phys. Rev. Lett. **91**, 125004 (2003).

[5] S. V. Bulanov and V. S. Khoroshkov, Plasma Phys. Rep. **28**, 453 (2002).

[6] S. C. Wilks, A. B. Langdon, T. E. Cowan, M. Roth, M. Singh, S. Hatchett, M. H. Key, D. Pennington, A. MacKinnon, and R. A. Snavely, Phys. Plasmas **8**, 542 (2001).

[7] S. C. Wilks and W. L. Kruer, IEEE J. Quantum Electron. **33**, 1954 (1997).

[8] P. Gibbon and E. Förster, Plasma Phys. Controlled Fusion **38**, 769 (1996).

[9] A. Maksimchuk, S. Gu, K. Flippo, D. Umstadter, and V. Yu. Bychenkov, Phys. Rev. Lett. **84**, 4108 (2000).

[10] Y. Oishi, T. Nayuki, T. Fujii, Y. Takizawa, X. Wang, T. Yamazaki, K. Nemoto, T. Kayoiji, T. Sekiya, K. Horioka, Y. Okano, Y. Hironaka, K. G. Nakamura, K. Kondo, and A. A. Andreev, Phys. Plasmas **12**, 073102 (2005).

[11] P. Mora, Phys. Rev. Lett. **90**, 185002 (2003).

[12] Y. Sentoku, V. Y. Bychenkov, K. Flippo, A. Maksimchuk, K. Mima, G. Mourou, Z. M. Sheng, and D. Umstadter, Appl. Phys. B: Lasers Opt. **74**, 207 (2002).

[13] J. Fuchs, P. Antici, E. d'Humières, E. Lefebvre, M. Borghesi, E. Brambrink, C. A. Cecchetti, M. Kaluza, V. Malka, M. Manclossi, S. Meyroneinc, P. Mora, J. Schreiber, T. Toncian, H. Pépin, and P. Audebert, Nat. Phys. **2**, 48 (2006).

[14] E. Lefebvre, N. Cochet, S. Fritzler, V. Malka, M.-M. Aléonard, J.-F. Chemin, S. Darbon, L. Disdier, J. Faure, A. Fedotoff, O. Landoas, G. Malka, V. Méot, P. Morel, M. Rabec Le Gloahec, A. Rouyer, Ch. Rubbelynck, V. Tikhonchuk, R. Wrobel, P. Audebert, and C. Rousseaux, Nucl. Fusion **43**, 629 (2003).

[15] J. Fuchs, C. A. Cecchetti, M. Borghesi, T. Grismayer, E. d'Humières, P. Antici, S. Atzeni, P. Mora, A. Pipahl, L. Romagnani, A. Schiavi, Y. Sentoku, T. Toncian, P. Audebert, and O. Willi, Phys. Rev. Lett. **99**, 015002 (2007).

[16] E. d'Humières, E. Lefebvre, L. Gremillet, and V. Malka, Phys. Plasmas **12**, 062704 (2005).

[17] E. Lefebvre and G. Bonnaud, Phys. Rev. E **55**, 1011 (1997).

[18] S. C. Wilks, W. L. Kruer, M. Tabak, and A. B. Langdon, Phys. Rev. Lett. **69**, 1383 (1992).

[19] A. J. Mackinnon, M. Borghesi, S. Hatchett, M. H. Key, P. K. Patel, H. Campbell, A. Schiavi, R. Snavely, S. C. Wilks, and O. Willi, Phys. Rev. Lett. **86**, 1769 (2001).

[20] T. Grismayer and P. Mora, Phys. Plasmas **13**, 032103 (2006).

[21] A. A. Andreev, R. Sonobe, S. Kawata, S. Miyazaki, K. Sakai, K. Miyauchi, T. Kikuchi, K. Platonov, and K. Nemoto, Plasma Phys. Controlled Fusion **48**, 1605 (2006).

[22] R. Nuter, L. Gremillet, P. Combis, M. Drouin, E. Lefebvre, A. Flacco, and V. Malka, J. Appl. Phys. **104**, 103307 (2008).

[23] G. Doumy, F. Quéré, O. Gobert, M. Perdrix, P. Martin, P. Audebert, J. C. Gauthier, J.-P. Geindre, and T. Wittmann, Phys. Rev. E **69**, 026402 (2004).

[24] A. Jullien, O. Albert, F. Burgy, G. Hamoniaux, J.-P. Rousseau, J.-P. Chambaret, F. Augé-Rochereau, G. Chériaux, J. Etchepare, N. Minkovski, and S. M. Saltiel, Opt. Lett. **30**, 920 (2005).

[25] L. Robson, P. T. Simpson, R. J. Clarke, K. W. D. Ledingham, O. Lundh, F. Lindau, T. McCanny, P. Mora, D. Neely, C.-G. Walhstrom, M. Zepf, and P. McKenna, Nat. Phys. **3**, 58 (2007).